

Inter-Laboratory Comparison of CMOS Distortion Measurements*

Kate A. Remley¹, Joe Gering², Susan Sweeney³, C. Michael Olsen⁴,
Cliff Xie², Dave Walker¹, Tom McKay⁵, Jack Pekarik³

¹Electromagnetics Division, National Institute of Standards and Technology, Boulder Colorado

²RF Micro Devices, Greensboro, NC

³IBM Semiconductor Research and Development Center, Essex Junction, VT

⁴IBM Semiconductor Research and Development Center, Hopewell Junction, NY

⁵RF Micro Devices, Scotts Valley, CA

Contact: remley@boulder.nist.gov

Abstract—We describe a measurement comparison of distortion in a complementary metal-oxide semiconductor low-noise device operating under weakly nonlinear conditions. Issues that commonly arise in performing and interpreting nonlinear measurements are discussed, such as power and wave-based representations and the effects of terminating impedance on intermodulation distortion. We demonstrate that the increased confidence provided by a measurement comparison can help to diagnose issues with a device model that was initially derived from DC I/V curves and their derivatives and then compared to RF measurement.

Key Words— CMOS device, large-signal network analyzer, load-pull system, low-noise amplifier, measurement-based modeling, measurement comparison, nonlinear measurements, wireless systems

I. INTRODUCTION

Accurate data on distortion behavior of nonlinear radio-frequency (RF) devices is a key element in understanding how the device will perform once it is incorporated into a system. Even under weakly nonlinear conditions, low-noise devices such as those used in receiver front ends will exhibit nonlinear behavior that includes harmonic generation and intermodulation distortion. Because many (CMOS) device models are extracted from DC I/V data, accurate measurements of RF distortion under realistic load and bias conditions can provide useful information to verify model performance.

We describe an interlaboratory measurement comparison carried out between NIST, IBM Microelectronics, and RF Micro Devices (RFMD). This work is an extension of the noise measurement comparison presented in [1]. The goal of the present measurement comparison was to enhance confidence in measurements of CMOS components for model development and verification, as well as for qualifying the performance of the components. Using standard techniques, we measured nonlinear circuits from the same wafer in the three different labs using two different classes of instruments: (1) load-pull systems and (2) large-signal network analyzers (LSNAs) [2]. Our comparison of measurements from these different instruments required that we consider several practical implementation issues in the nonlinear measurement environment. After describing the instrumentation, we detail some of the implementation issues below. We follow with an example where our measurement comparison helped to resolve questions regarding model verification for a representative low-noise CMOS device model.

Presented at the 69th ARFTG Microwave Measurement Conference, May 2009

* Partial work of the U.S. government, not subject to copyright in the United States.

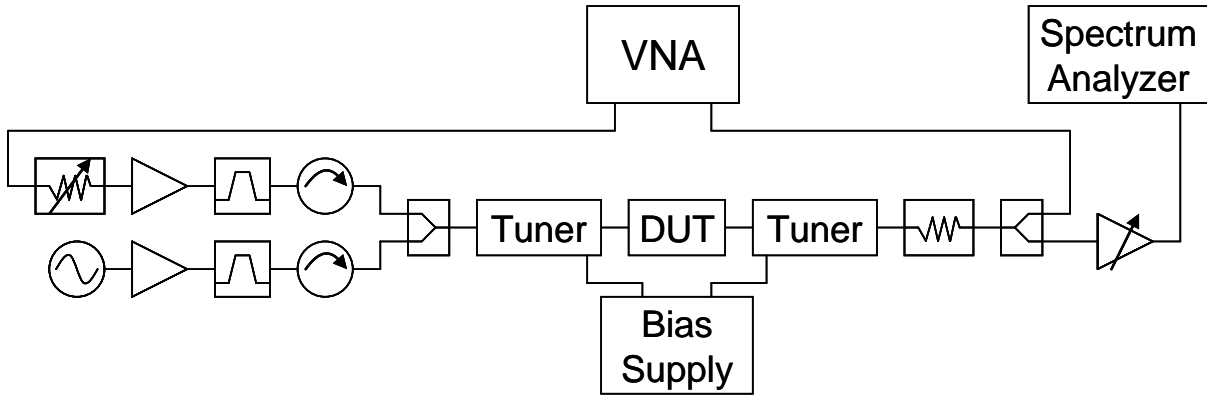
II. INSTRUMENTATION USED IN THE DISTORTION MEASUREMENTS

We used instruments that measure the nonlinear distortion characteristics of a device, including harmonic generation and intermodulation distortion (IMD). These instruments included two load-pull systems that were used to measure only power and two large-signal network analyzers that are capable of vector measurements.

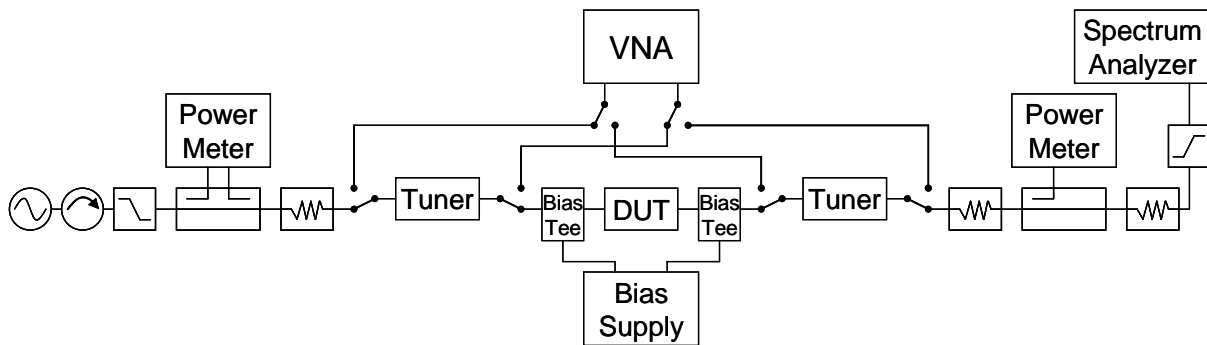
A. The Load-Pull Systems: Two different load-pull systems were used in our comparison. A simplified block diagram of the load-pull system used by IBM is shown in Figure 1(a). With this system, the VNA was used as one microwave source as well as a fast, high-dynamic-range, fundamental receiver. For two-tone measurements, a second source was combined with the VNA signal. The spectrum analyzer was used to measure all harmonics during single-tone measurements as well as all tones (fundamental, intermodulation products, and harmonics) in two-tone measurements. The tuners are electronic-tuner modules, and the bias tees are incorporated into the tuners. Deembedding was carried out to the on-wafer reference planes of the device by use of the techniques described in Refs. [3,4].

The system used by RFMD is a custom load-pull system for single-tone measurements only. Its simplified block diagram is given in Figure 1(b). This system is configured with manual tuners, so a VNA is incorporated into the system and is switched in to measure the source and load impedances once the device under test (DUT) is tuned for optimal performance. The power at the fundamental frequency is measured with the power meters, and the power at the harmonics is measured with the spectrum analyzer. This system uses discrete bias tees that are placed close to the DUT for better device stability, but at the expense of tuning range.

Both load-pull systems were configured for on-wafer measurements with RF probes contacting the DUT, and both systems are fully automated. With the IBM system, a single calibration procedure steps the user through the necessary S-parameter and power calibrations to determine all possible source and load impedances at the DUT reference plane as well as the loss correction factors to the measurement instruments. With the RFMD system, the S-parameters of certain blocks (for example the couplers, the switch networks, and the bias tee / RF probe combinations) are measured before the fact. These S-parameters are combined with the measurements of the tuners made after device tuning and provide the source and load impedance information as well as the necessary power loss correction factors to the measurement instruments. For both systems, after the characterization and calibration steps are performed, the systems report the power available from the source and the power delivered to the load at the on-wafer, DUT reference plane.



(a)



(b)

Figure 1: Simplified block diagrams of the load-pull systems used by (a) IBM and (b) RFMD for the measurement comparison. With both systems, after calibration, the systems report the power delivered to the load versus the power available from the source both at the DUT reference plane. Both systems can vary both the source and load impedance presented to the DUT.

B. The Large-Signal Network Analyzers: The LSNA uses sampling downconversion [5] to simultaneously acquire the fundamental and harmonics present at the input and output ports of a nonlinear circuit. Figure 2 shows a simplified block diagram of the NIST and RFMD LSNA's. Using couplers, the receiver measures the forward and reflected waves separately. Unlike with a vector network analyzer, the absolute magnitude of the fundamental and harmonic waves are measured, not the relative amplitudes. Unlike with a spectrum analyzer, the incident and reflected traveling voltage waves are measured, not the power. The phases of the harmonics relative to the fundamental are also acquired.

The LSNA's we used have two modes of operation, one for single-tone measurements and one for modulated-signal measurements. Both modes use the same acquisition hardware. The differences lie in the experiment design and in the instrument's processing. In the modulated-signal mode, the frequencies representing the excitation tones and the distortion products that lie near the fundamental and harmonics must be known and the system programmed to acquire them. The set-up and processing for this mode is more involved than for single-tone measurements.

The LSNAs we used had an upper frequency of 20 GHz and a modulation bandwidth of either 8 MHz (NIST) or 20 MHz (RFMD). Deembedding was carried out to the on-wafer reference planes of the CMOS device, again using the techniques described in Refs. [3,4] but also using the fixture deembedding procedure described in Ref. [6].

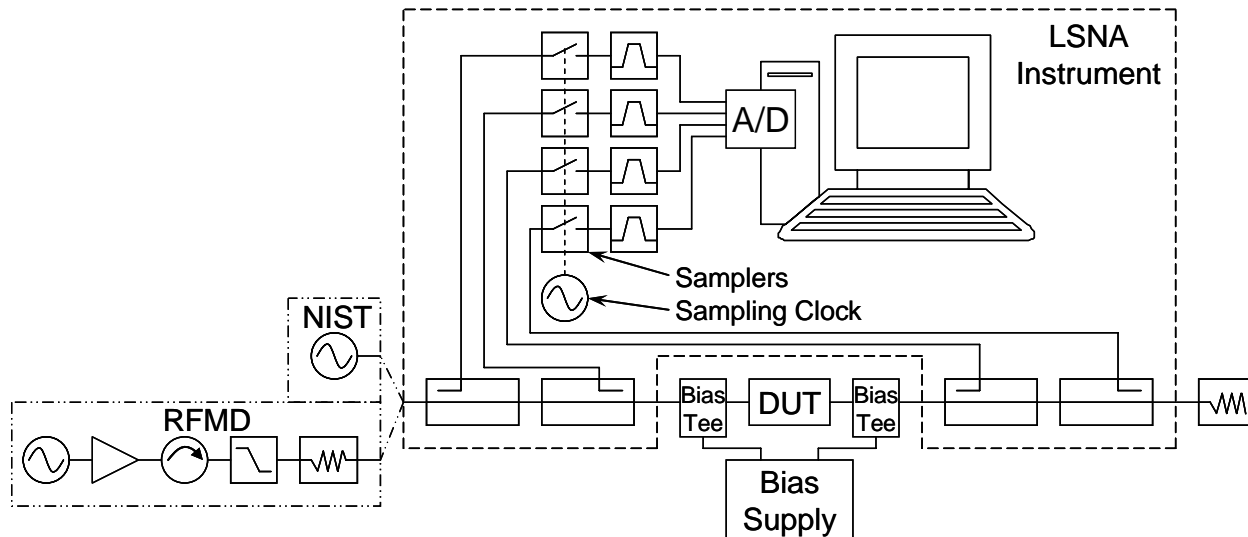


Figure 2: Simplified block diagram of the LSNAs used by NIST and RFMD. The schematic shows that the incident and reflected traveling waves are measured separately through couplers on either side of the DUT. Also shown are the sampling down-converters that enable simultaneous measurement of the fundamental and harmonics of a nonlinear circuit. The IF filters to the right of the samplers prevent aliasing of the down-converted signal, but also limit the modulation bandwidth to 8 MHz (NIST system) or 20 MHz (RFMD system). Also shown are the different source configurations used by NIST (source only) and RFMD (source-amplifier-isolator-filter-pad).

III. IMPLEMENTATION OF THE MEASUREMENT COMPARISON

A. Experiment design: One goal of the measurement comparison was to provide assurance that distortion data acquired from the CMOS device could ultimately be used, among other things, to verify a modeled result. Because the end use of the device is in a receiver front end, we focused on device behavior in the weakly nonlinear regime; that is, at input power levels several decibels below the compression point of the device. We first swept the input power from -40 dBm to $+10$ dBm to ascertain the weakly nonlinear regime for this device. The range between -30 dBm and -10 dBm was sufficiently above the noise floor of the measurement instruments and low enough that significant compression was not observed. We carried out both single-tone and two-tone power sweeps within these input power ranges with the devices terminated nominally in 50Ω . Because this comparison involved nonlinear circuits, the absolute input power levels had to be characterized carefully through calibration and deembedding techniques.

The $0.12\ \mu\text{m}$ CMOS devices we measured were all fabricated on the same wafer, as described in [1]. For the measurements, the devices were biased to a drain voltage of $1.2\ \text{V}$. The gate voltage

was adjusted such that the drain current was 9.6 mA under small-signal conditions and was allowed to increase as the device self-biased at higher input signal levels.

We measured second- and third-harmonic generation in the weakly nonlinear regime. We also measured intermodulation products, specifically IM3 (at frequencies $2\omega_1 - \omega_2$ and $2\omega_2 - \omega_1$), IM5 (at frequencies $3\omega_1 - 2\omega_2$ and $3\omega_2 - 2\omega_1$), and in some cases IM7 (at frequencies $5\omega_1 - 4\omega_2$ and $5\omega_2 - 4\omega_1$), where ω_1 and ω_2 are the two fundamental excitation tones.

Note that none of the instruments we used have measurement uncertainties associated with them. Thus the measurement comparison presented here can provide measurement assurance, but not a real assessment of measurement accuracy. The focus of this paper is, rather, to discuss practical implementation issues that must be considered when carrying out a nonlinear measurement comparison.

B. Wave and power representations

We needed to convert between the incident and reflected traveling-wave representation provided by the LSNA and the power-based representation of the load-pull systems. To perform a direct comparison of the distortion measurements from the LSNA and load-pull systems, we first transformed the incident and reflected waves to a voltage and current representation, and from this we calculated the total power transmitted across the reference plane.

The manufacturers of the LSNA define the (voltage) traveling waves with respect to a 50 Ω reference impedance [6]. The transformation between the incident (a) and emanating (b) traveling waves and the voltage (v) and current (i) in this voltage-wave normalization is given by

$$v_k = a_k + b_k, \text{ and } i_k = \frac{a_k - b_k}{50}, \quad (1)$$

where the subscript k refers to port number one or two, which are the input and output ports, respectively. Here the current is defined going into the DUT. From this, we calculate power delivered to the load as

$$P_{\text{load}} = \frac{1}{2} \text{Re}[v_2(-i_2^*)] = \frac{|b_2|^2 - |a_2|^2}{2 \times 50}, \quad (2)$$

where the * symbol denotes the complex conjugate, and the wave version is possible because the traveling waves are defined with a 50 Ω reference impedance. The equation for the available power from the source can be calculated as

$$P_{\text{avs}} = \frac{\left|1 - \Gamma_S \frac{b_1}{a_1}\right|^2 \frac{|a_1|^2}{2 \times 50}}{1 - |\Gamma_S|^2}, \quad (3)$$

where Γ_S is the reflection coefficient of the source.

Note that (1) – (3) describe power calculations for a single tone. To calculate powers involving multiple tones, harmonics, and intermodulation products, we need to calculate the measured power in each tone with Equations (1) – (3) and sum the results.

C. Distortion in the signal generator: We measured the harmonic distortion of the two different vector signal generators used in the LSNA measurements. The generators were terminated in the broadband $50\ \Omega$ impedance presented by the LSNA by measuring a thru. The results in Figure 3 show a noticeable increase in second-harmonic distortion for the NIST vector signal generator for input powers greater than about $-10\ \text{dBm}$. The harmonic distortion from the RFMD generator is significantly lower, in part because the signal output from this unit passes through a low-pass filter before being measured, as shown in Figure 2.

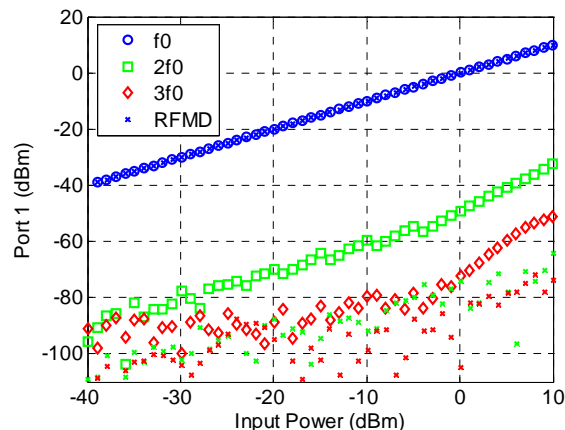


Figure 3: Measured output of the vector signal generators used in the two LSNA systems when terminated in $50\ \Omega$. The NIST unit’s output is represented by various open symbols, while the RFMD unit’s output is given by x’s. The second harmonic distortion of the NIST unit is approximately $-60\ \text{dBm}$ when the generator is set to $-10\ \text{dBm}$. The output of the RFMD unit passes through a low-pass filter before being measured, and this significantly reduces the harmonic distortion. This measurement helped to determine the valid input signal range for the measurement comparison.

Our measurement comparison was carried out in the weakly nonlinear regime between input powers of $-30\ \text{dBm}$ and $-10\ \text{dBm}$. For this range, the distortion products emanating from the CMOS device were generally higher than those of the signal generators, and we anticipated that the signal generator distortion should have no significant impact on the measurement comparison results. However, lack of an uncertainty analysis hampers any quantifiable statements in this regard.

D. Terminating impedance: We first considered the terminating impedance at RF. The terminations at the harmonic frequencies had a significant effect on the magnitude and phase of the nonlinear mixing products at the harmonics. Figure 4(a) illustrates this effect. Here we see a comparison of harmonic distortion measurements carried out with the NIST LSNA and the IBM load-pull system. In the latter system, the second and third harmonic terminations first have significant reactive components (dotted line) and then are terminated in approximately $50\ \text{ohms}$ (solid line). Figure 4(b) shows the values of the terminating impedances at the fundamental, second, and third harmonics. To allow for a proper comparison of the CMOS device harmonic

distortion, we ensured that all systems presented a near $50\ \Omega$ load impedance at the fundamental and higher harmonics.

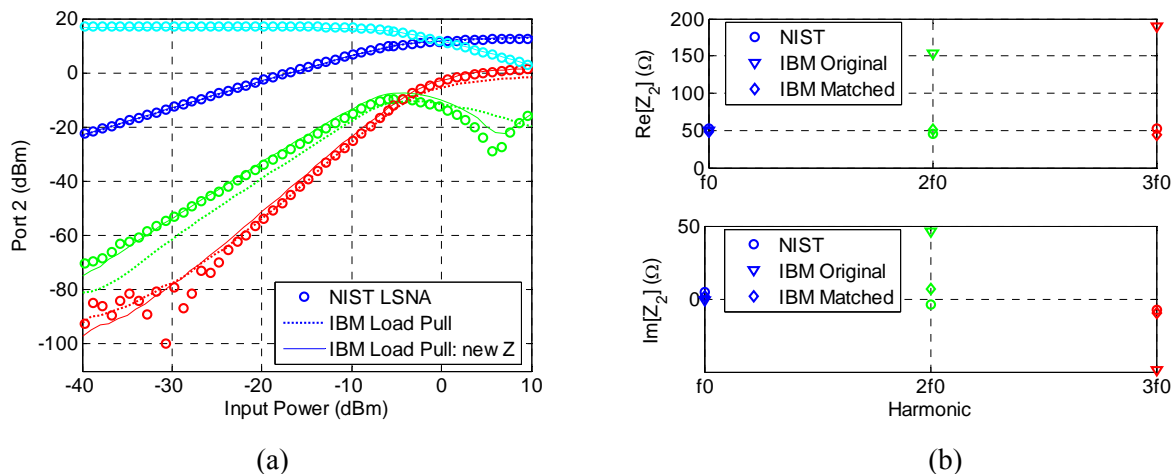


Figure 4: Harmonic distortion measurements carried out on the NIST LSNA and the IBM load-pull systems. From top curve to bottom curve in (a): gain, f_0 , $2f_0$, $3f_0$. The LSNA has a broadband $50\ \Omega$ termination. The IBM system initially used reactive second and third harmonic terminations (dotted line in (a), inverted triangles in (b)) and subsequently used real, $50\ \Omega$ second and third harmonic terminations (solid line in (a), diamonds in (b)).

For the two-tone measurements, the issue of terminating impedance is further compounded. Not only is the termination at the harmonics important, but the termination presented to the DUT at the baseband frequencies is also important. For a two-tone measurement, the baseband is defined as the difference frequency between the tones (1 MHz in our case) and the harmonics of this difference frequency. A reactive impedance at baseband can introduce into the passband of the device additional intermodulation distortion, so-called “memory effects” [7, 8].

The baseband termination is often heavily determined by the bias tee, cabling, and DC power supply used in the measurement systems [7, 8]. Figure 5 shows the low-frequency impedance presented to the DUT for the RFMD LSNA and the IBM load-pull measured directly with a low frequency VNA. While the curves for both systems show the same basic behavior, the actual impedances are quite different from each other and are both different from $50\ \Omega$. The traces of Figure 5 depend on the power supplies being set to the same ranges and compliances (and turned on) as in the device measurements. As described below in Section IV, our current approach for using the data from the measurement comparison to validate a device model is to match the baseband impedance of a simulation to the baseband impedance of the measurement system. In the future, we hope to investigate low frequency by-passing that will allow all systems to present similar baseband impedances.

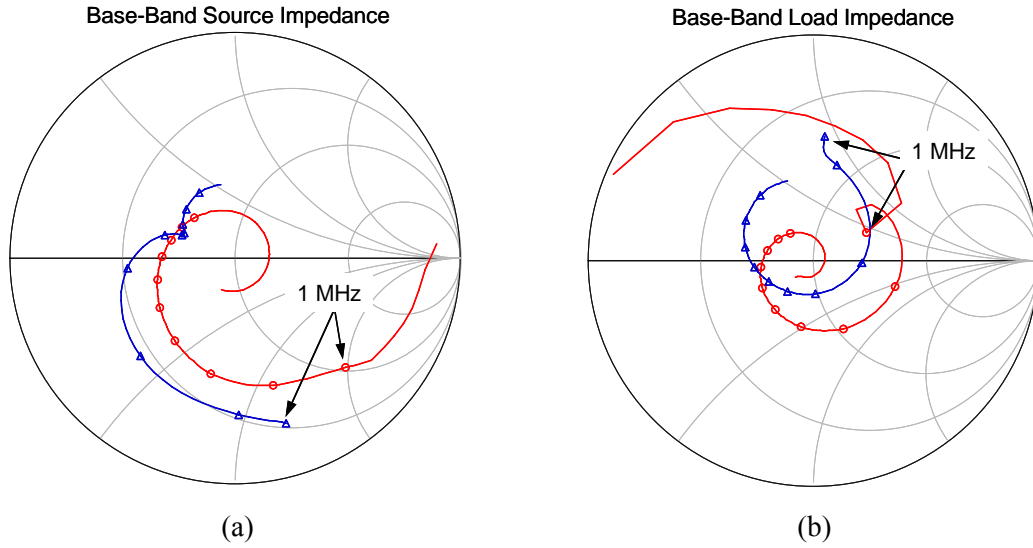


Figure 5: Baseband impedance presented to (a) port 1 of the DUT and (b) port 2 of the DUT for the RFMD LSNA (circles) and IBM load-pull (triangles). The symbols mark 1, 2, ..., 10 MHz.

E. Measurement comparison results: Figure 6 shows the results of our measurement comparison for single-tone power sweeps of the CMOS device. Figure 6(a) shows the magnitude of the measured frequency components at the output reference plane of the device. Figure 6(b) zooms in to show the second and third harmonics in the weakly nonlinear regime between -30 and -10 dBm input power.

Differences between the various measurement systems are given in Table I. These are not normalized quantities, but rather absolute powers. As such, the agreement is quite good, considering the differences in embedding impedances including the different bias tees, and the fact that the devices we measured were similar but not the same. As can be seen in the table, for input powers of -30 dBm and lower, the noise floor of the LSNAs and the RFMD load-pull became an issue.

Figure 7 shows the measured results of two-tone power sweeps carried out on the NIST LSNA, the RFMD LSNA, and the IBM load-pull system. Intermodulation distortion is plotted up to the seventh IM product. Figure 7(a) shows the fundamental tones and the intermodulation distortion products over the full range of input powers, and Figure 7(b) shows the IM products in the weakly nonlinear regime.

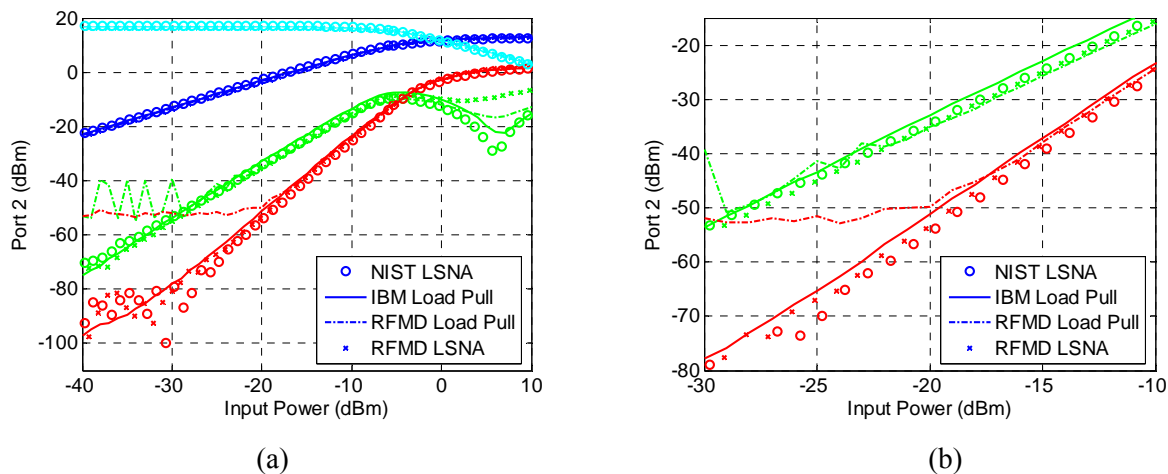


Figure 6: A four-way measurement comparison of harmonic distortion under single-frequency excitation for a CMOS low-noise device at (a) the full range of input powers. From top curve to bottom curve in (a): gain, f_0 , $2f_0$, $3f_0$; the systems have nearly 50Ω terminations. In (b), the weakly nonlinear regime of interest is enlarged. The top curve is for $2f_0$ and the bottom curve is for $3f_0$. At an input power level of -10 dBm the LSNA systems agree to within 1.0 dB for the second harmonic and 3.1 dB for the third harmonic. At an input power level of -10 dBm the load-pull systems agree to within 2.7 dB for the second harmonic and 1.3 dB for the third harmonic.

Table I: The difference in magnitudes of the second and third harmonics at specific input power levels in the weakly nonlinear regime, as measured by the instruments.

Difference between NIST and RFMD LSNAs			Difference between IBM and RFMD load-pull systems			Difference between NIST LSNA and IBM load-pull		
Input power	$2f_0$ (dB)	$3f_0$ (dB)	Input power	$2f_0$ (dB)	$3f_0$ (dB)	Input power	$2f_0$ (dB)	$3f_0$ (dB)
-10 dBm	0.9	3.1	-10 dBm	2.7	1.0	-10 dBm	3.1	4.2
-20 dBm	0.5	2.9	-20 dBm	2.1	1.3	-20 dBm	2.9	5.5
-30 dBm	1.8	5.9	-30 dBm	--	--	-30 dBm	0.5	1.2

The plots show little difference between the upper and lower measured components; thus we do not distinguish between the IBM and RFMD data. Note that at the lower input power levels, the measurements from the LSNA systems exhibit a significant random component due to the lower dynamic range of these systems relative to the load-pull systems. In fact, because of the noise floor issues and the harmonic distortion present in the NIST signal generator, the agreement between the IM5 measurements above -13 dBm is surprisingly good.

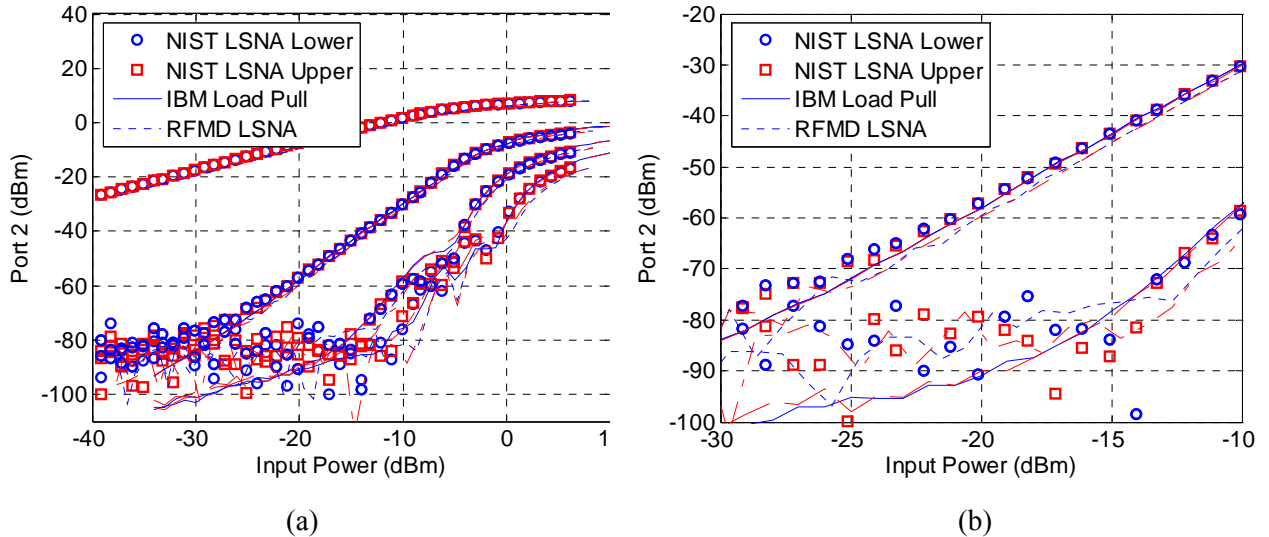


Figure 7: Measured results of the output power for a two-tone power sweep using the NIST LSNA (symbols), the IBM load-pull system (solid lines), and the RFMD LSNA (dashed lines). The upper and lower input frequencies, IM3, IM5, and IM7 intermodulation products are shown in curves from top to bottom, respectively, for (a) the full range of input powers and (b) the weakly nonlinear regime. At -10 dBm input power, the agreement between the LSNA measurements and the load-pull measurements is within 0.5 dB for IM3 and 2 dB for IM5.

IV. APPLICATION OF THE MEASUREMENT COMPARISON TO MODELING A LOW-NOISE CMOS DEVICE

We applied the results of our measurement comparison to the verification of a $0.12 \mu\text{m}$ CMOS RF foundry device model. The model is based on the BSIM4 MOSFET model. Simulations were done with a commercial RF simulator. We discovered disagreement between the measured and simulated IV curves, so the model parameters were recentered using the measured DC $I_d V_g$ and $I_d V_d$ data and their derivatives. Before and after results of the parameter adjustment can be seen in Figure 8 for the $I_d V_g$ data. The purpose of readjusting the parameters is to enable a better prediction of distortion under AC operation.

After the I/V recentering, we noticed that the simulated S_{21} was 0.5 dB below the measured S_{21} from 1.8 to 8.0 GHz. Since S_{21} significantly affects IM3, we also recentered the C/V parameter set, though not as comprehensively as the I/V recentering. Basically, a slight adjustment was made to two overlap capacitance parameters. We then checked if this adjustment disturbed the quality of the small-signal S -parameter fits. While the fitting of magnitudes of S -parameters did not change noticeably, the phase of S_{11} , S_{12} , and S_{21} did change by a few degrees with S_{11} impacted the most. This issue will be investigated further from a compact modeling point of view to find out if within BSIM4 we can find a set of parameters to simultaneously fit the DC characteristics, small-signal S -parameters, and large-signal characteristics.

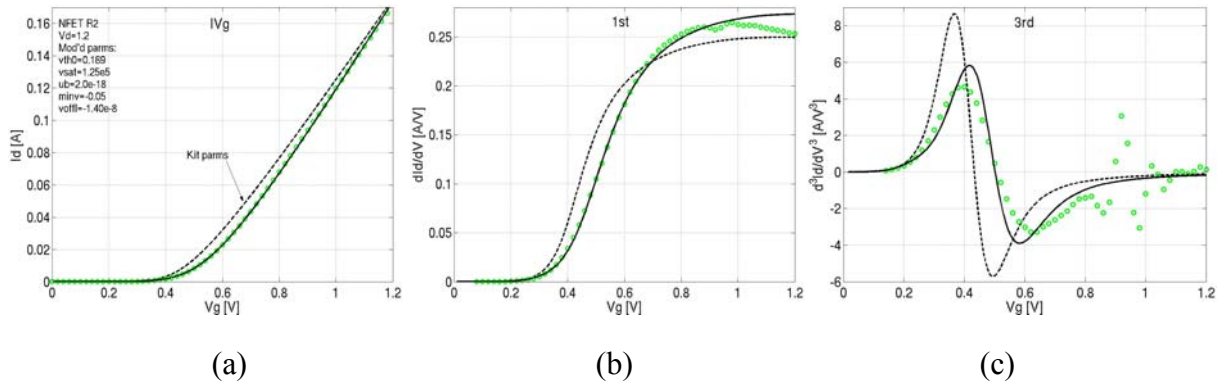


Figure 8: Measured and simulated drain current, first, and third derivatives as a function of V_g . Symbols are measured data, dashed lines represent default library parameters, and solid lines are after a readjustment (recentering) of the library parameters.

Figure 9 compares distortion measurements made on the IBM load-pull system and a simulation made with the recentered model parameters. Harmonics are shown by the dashed lines and intermodulation distortion is shown by the solid lines. In Figure 9(a), we see that the match between simulations and measurements is generally good throughout the power range. Even IM5 matches surprisingly well including a reasonable prediction of the sweep spot. However, the difference between simulation and measurement for the IM3 product is greater than the differences obtained in our measurement comparison. As shown in the inset of Figure 9(a), the difference between measured and simulated IM3 was approximately 4 dB at -25 dBm input power, while the difference between measured IM3 values was closer to 1 dB. Since the first three harmonics are predicted well, we felt that the recentered model performed satisfactorily and that the explanation for the IM3 mismatch lay elsewhere, for example at the baseband frequencies.

In our simulations we used a simple LC model for the bias tees. The bias tee model used for Figure 9(a) produced a ~ 5 dB drop in simulated Γ_L at 45 MHz with typical circuit parameter values of a representative bias tee. In Figure 9(b), we revised the bias tee model to better approximate the baseband impedance of the IBM load-pull system bias tees. Better agreement between simulated and measured IM3 (approximately 2 dB difference at -25 dBm input power versus 4 dB previously) was achieved with this improved model of the bias tee. Obviously an adequate representation of the bias tee characteristics is of great importance and is being investigated. The sensitivity of the IM3 response to the bias tee is probably an indication of memory effects. Refs. [7, 8] indicate that reactive loads may cause significant memory effects in the IM3 response.

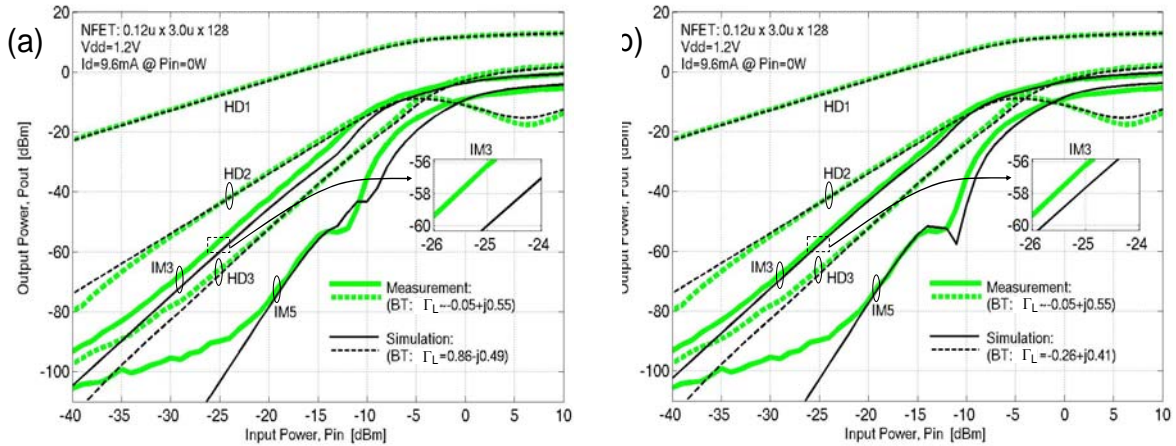


Figure 9: Comparison of measurement (thick, lighter-colored lines) and simulation (thin, black lines) for a low-noise $0.12 \mu\text{m}$ CMOS NFET device. In (a), simulated results used a simple model of a representative bias tee that produces a simulated $\Gamma_L = 0.86 - j0.49$ at 1 MHz. In (b), simulated results used the same bias tee circuit model but with L and C chosen to produce $\Gamma_L = -0.26 + j0.41$ for a better match to the measured $\Gamma_L = -0.05 + j0.55$ at 1 MHz. Shown are the fundamental (HD1), second (HD2) and third (HD3) harmonics and the third (IM3) and fifth (IM5) intermodulation products. Two tones at 1.8 GHz and 1.801 GHz were supplied at the amplifier input. HD1, HD2 and HD3 were obtained from single tone excitation. Simulated source and load impedances were 52.5Ω and 51.5Ω at the fundamental, respectively. BT stands for bias tee.

V. CONCLUSION

In this paper, we described a measurement comparison carried out between four measurement systems on a low-noise CMOS device operating in the weakly nonlinear regime. The goal of the measurement comparison was to enhance measurement confidence in the participants' nonlinear distortion measurements for use in model verification. Even though only qualitative comparisons could be conducted, due to lack of uncertainty bounds on the measurements, we were able to utilize the measurement comparison results to diagnose model extraction issues. By process of elimination, since our measurements agreed well, we suspected the model or simulation needed to be refined. In this instance, the impact of the bias tee on the simulated IM3 response was demonstrated. The bias tee must be adequately represented in the simulation due to its memory effects on the IM3 data.

Several practical issues in implementing a nonlinear measurement comparison were discussed. These issues include whether the instrument represents the measurement as a voltage or a wave, the impedance environment in which the device is measured, the distortion in the excitation source, and the DC bias circuit.

This effort has established multiple lab correlation and quantified required control of factors such as harmonic termination and baseband impedance needed to obtain agreement. The focused model and simulation effort has shown that the weakly nonlinear regime for a $0.12 \mu\text{m}$ NMOS device biased in weak inversion can be predicted using existing models with some adjustments to the extraction procedure. Given this baseline of repeatable experiment and consistent simulation, we are now in position to apply the methods to extend the bias coverage, consider additional

device configurations, verify strongly nonlinear regions of operation and move to multi-tone excitation representative of spectrally efficient modulation formats such as OFDM and WCDMA.

ACKNOWLEDGEMENT

The authors would like to acknowledge contributions to this project from other members of the Kelvin collaboration, including G. Ali Rezvani, Leonard Reynolds, and Dave Halchin of RFMD, David Greenburg and Lawrence Wagner of IBM, and James Randa of NIST.

REFERENCES

- [1] J. Randa, S.L. Sweeney, T. McKay, D.K. Walker, D.R. Greenburg, J. Tao, J. Mendez, G. A. Rezvani, J.J. Pekarik, "Interlaboratory comparison of noise-parameter measurements on CMOS devices with 0.12 μ m gate length," *66th ARFTG Conf. Dig.*, Washington, D.C., Dec. 2005, pp. 77-81.
- [2] J. Verspecht, P. Debie, A. Barel, and L. Martens, "Accurate on wafer measurement of phase and amplitude of the spectral components of incident and scattered voltage waves at the signal ports of a nonlinear microwave device," *IEEE MTT-S Int. Microwave Symp. Dig.*, pp. 1029-1032, 1995.
- [3] R.B. Marks and D.F. Williams, "Characteristic impedance determination using propagation constant measurement," *IEEE Microwave and Guided Wave Lett.*, vol.1, no. 6, pp. 141-143, June 1991.
- [4] D.F. Williams and R.B. Marks, "Transmission line capacitance measurement," *IEEE Microwave and Guided Wave Lett.*, vol.1, no. 9, pp. 243-245, Sept. 1991.
- [5] J. Verspecht, "The return of the sampling frequency convertor," *62nd ARFTG Conf. Dig.*, Boulder, CO, Dec. 2004, pp. 155-161.
- [6] NMDG Engineering, "Maury Microwave Large-signal network analyzer user's guide, MT4463 Series," 2004. Specification of this product does not constitute endorsement by NIST or the U.S. government. Other products may work as well or better.
- [7] N. Borges de Carvalho and J. C. Pedro, "A comprehensive explanation of distortion sideband asymmetries," *IEEE Trans. Microwave Theory Tech.*, vol. 50, pp. 2090–2101, Sept. 2002.
- [8] K.A. Remley, D.F. Williams, D.M.M-P. Schreurs, and J. Wood, "Simplifying and interpreting two-tone measurements," *IEEE Trans. Microwave Theory Tech.*, vol. 52, no. 11, Nov. 2004, pp. 2576-2584.